# Complementary and divergent functions of zebrafish Tango1 and Ctage5 in tissue development and homeostasis

Eric M. Clark and Brian A. Link*
Department of Cell Biology, Neurobiology and Anatomy, Medical College of Wisconsin, Milwaukee, WI 53226

**ABSTRACT** **Coat protein complex II (COPII) factors mediate cargo export from the endoplasmic reticulum (ER), but bulky collagens and lipoproteins are too large for traditional COPII vesicles. Mammalian CTAGE5 and TANGO1 have been well characterized individually as specialized cargo receptors at the ER that function with COPII coats to facilitate trafficking of bulky cargoes. Here, we present a genetic interaction study in zebrafish of deletions in *ctage5*, *tango1*, or both to investigate their distinct and complementary potential functions. We found that Ctage5 and Tango1 have different roles related to organogenesis, collagen versus lipoprotein trafficking, stress-pathway activation, and survival. While disruption of both *ctage5* and *tango1* compounded phenotype severity, mutation of either factor alone revealed novel tissue-specific defects in the building of heart, muscle, lens, and intestine, in addition to previously described roles in the development of neural and cartilage tissues. Together, our results demonstrate that Ctage5 and Tango1 have overlapping functions, but also suggest divergent roles in tissue development and homeostasis.**

**Monitoring Editor**
Benjamin Glick
University of Chicago

Received: Nov 24, 2020
Revised: Dec 24, 2020
Accepted: Jan 5, 2021

## INTRODUCTION

Secretory proteins are trafficked by coat protein complex II (COPII) vesicles that form at specialized sites of the endoplasmic reticulum (ER) called ER-exit sites (ERES; Bonifacio and Glick, 2004; Lee *et al.*, 2004). These sites contain conserved proteins such as SEC12, SEC16, SEC13, SEC31, SEC23, SEC24, and SAR1, among others that are important for COPII-mediated trafficking (Sato & Nakano, 2005; Watson *et al.*, 2006; Townley *et al.*, 2008; Kim *et al.*, 2012; Saito *et al.*, 2014; Maeda *et al.*, 2017). Some bulky molecules are too large to fit into traditional COPII vesicles, which are 60–90 nm (Miller and Schekman, 2013; Malhotra and Erlman, 2015). Recently, a transport system using specialized cargo receptors, the CTAGE5 (MEA6)/TANGO1(MIA3) family, has been described for large molecules such as collagens, chylomicrons, and very–low density lipoproteins (VLDLs; Saito *et al.*, 2009; Saito *et al.*, 2011; *Wilson et al.*, 2011; Maeda *et al.*, 2016; Maiers *et al.*, 2016; Santos *et al.*, 2016; Rios-Barrera *et al.*, 2017).

Evolution has created significant diversity in the CTAGE5/TANGO1 protein families. The human CTAGE5 and TANGO1 family is transcribed at the *MIA2* and *MIA3* gene loci, respectively. The *MIA2* locus transcribes *MIA2, CTAGE5, and TALI* isoforms and the

This article was published online ahead of print in MBoC in Press (http://www.molbiolcell.org/cgi/doi/10.1091/mbc.E20-11-0745) on January 13, 2021.

Competing financial interests: The authors declare no competing financial interests.

Author contributions: E.M.C. and B.A.L. designed the experiments. E.M.C. performed and analyzed the experiments. E.M.C. and B.A.L. wrote the manuscript and read and approved the final manuscript.

*Address correspondence to: Brian A. Link (blink@mcw.edu).

Abbreviations used: APOB, apolipoprotein B; ATF4, activating transcription factor 4; ATF6, activating transcription factor 6; BODIPY, boron-dipyrromethene; BSA, bovine serum albumin; CAS9, CRISPR associated protein 9; COPII, coat protein complex II; CRISPR, clustered regularly interspaced short palindromic repeats; CTAGE5, cutaneous T-cell lymphoma-associated antigen 5; D2GFP, destabilized green fluorescent protein; DAPI, 4′,6-diamidino-2-phenylindole; DEPC, diethyl pyrocarbonate; $dH_2O$, distilled $H_2O$; DMSO, dimethyl sulfoxide; DNA, deoxyribonucleic acid; DPF, days post-fertilization; EMBL-EBI, European bioinformatics institute; ER, endoplasmic reticulum; ERES, endoplasmic reticulum exit sites; ERGIC, endoplasmic reticulum Golgi intermediate compartment; GAP43, growth associated protein 43; gDNA, genomic deoxyribonucleic acid; gRNA, guide ribonucleic acid; GWAS, genome-wide association study; MIA, melanoma inhibitory activity; mRNA, messenger ribonucleic acid; NGS, normal goat serum; PACT, passive clarity technique; PBS, phosphate buffered saline; PCR, polymerase chain reaction; PERK, PKR-like endoplasmic reticulum kinase; PFA, paraformaldehyde; PTU, 1-phenyl 2-thiourea; RNAseq, ribonucleic acid sequencing; SAR1, secretion associated RAS related GTPase 1; SAR1, secretion-associated RAS-related 1; scRNAseq, single cell ribonucleic acid sequencing; TALI, TANGO-like; TANGO1l, transport and Golgi organization protein 1 long; TANGO1s, TANGO1 short; TUNEL, terminal deoxynucleotidyl transferase biotin-dUTP nick end labeling; UPR, unfolded protein response; VLDL, very-low density lipoprotein; XBP1, x-box binding protein 1; ZDR, zebrafish Danio rerio.

*MIA3* locus transcribes *TANGO1S* (short) and *TANGO1L* (long) isoforms (reviewed in McCaughey and Stephens, 2019). Human and mouse studies have suggested that *CTAGE5* and *TANGO1L* are expressed ubiquitously, whereas *MIA2* and *TALI* expression are more limited, based on tissue transport requirements (Pitman *et al.*, 2011; Santos *et al.*, 2016). TANGO1S was only recently characterized (Maeda *et al.*, 2016) and its expression across tissues is still unknown. Ensemble transcript analysis revealed that the zebrafish *mia2* gene locus only transcribes *ctage5* (*mia2*-205) and the *mia3* gene locus transcribes *tango1s (mia3*-201) *and tango1l* (*mia3*-202; Supplemental Figure S1). The simplified protein diversity of Ctage5/Tango1 in zebrafish compared with humans allows investigation of their complementary and divergent functions. In the current study, we specifically investigate deletion of *ctage5* and *tango1l* separately and together.

Members of the CTAGE5/TANGO1 family form a ring-like structure at the base of ERES vesicles and promote their expansion to accommodate large cargo (Lui *et al.*, 2017; Raote *et al.*, 2017; Reynolds *et al.*, 2019) or potentially facilitate defined tubular connections for transfer of material to the cis-Golgi (Kurokawa *et al.*, 2014; Raote and Malhotra, 2019; Raote *et al.*, 2020). In vitro studies have suggested some redundant functions of the CTAGE5/TANGO1 family for transport of some collagens (Maeda *et al.*, 2016), but unique functions for trafficking others (Santos *et al.*, 2016). The families may also act cooperatively for transport of other large molecules such as VLDLs and chylomicrons (Santos *et al.*, 2016). In vivo studies of TANGO1/CTAGE5 family members have been relatively limited, likely because in mice *Tango1* deletion is perinatally lethal (Wilson *et al.*, 2011) and *Ctage5* deletion is essential for early embryonic development (Wang *et al.*, 2016). *Tango1l* deletion caused buildup of multiple collagen subtypes in chondrocytes, fibroblasts, endothelial cells, and mural cells (Wilson *et al.*, 2011). Conditional knockout of *Ctage5* in neurons of mice show that in addition to secretory components, nonsecretory protein trafficking is also affected (Zhang *et al.*, 2018). Similarly, *Drosophila* studies have shown that secretion of multiple extracellular proteins including mucins, laminins, and perlecan is disrupted after loss of Tango1 (Petley-Ragan *et al.*, 2016; Liu *et al.*, 2017; Rios-Barrera *et al.*, 2017; Reynolds *et al.*, 2019). The specific mechanisms underlying the broad disruption of ER trafficking are still being investigated. Of significance, however, studies of *Ctage5* and *Tango*1 deletions within a single animal model have not been reported, highlighting a need to investigate their potential redundancies or unique functions in different cell types.

When trafficking dynamics is altered at the endoplasmic reticulum, stress pathways within the cell can be activated (Walter and Ron, 2011). This coordinated response has three major branches: the ATF6, PERK, and XBP1 pathways. After TANGO1 knockdown, the ER is distended (Wilson *et al.*, 2011; Petley-Ragan *et al.*, 2016; Rios-Barrerra *et al.*, 2017; Maiers *et al.*, 2016) and XBP1 and ATF4 ER stress pathways are activated, but ATF6 was not investigated (Maiers *et al.*, 2016; Petley-Ragan *et al.*, 2016). CTAGE5 KO can also cause ER stress in pancreatic islets (Fan *et al.*, 2017). With buildup of material at the ER and ER stress, autophagy is also commonly activated (Kabir *et al.*, 2018). After loss of TANGO1 in HEPG2 or Caco-2 cells, APOB accumulates intracellularly and is targeted for lysosomal degradation (Santos *et al.*, 2016). Furthermore, CTAGE5 was shown as essential for starvation-induced autophagosome formation in HeLa cells, acting at the ERES for membrane donation (Ge *et al.*, 2017). The role of TANGO1, however, was not investigated in that study. Interestingly, noncanonical autophagy can directly remove collagen from ERESs to maintain homeostasis (Omari *et al.*, 2018). Cumulatively, the literature suggests that protein trafficking and membrane donation functions of Ctage5 and Tango1 could be closely related to stress pathway activation and cellular homeostasis (McCaughey and Stephens, 2019).

Zebrafish have been used previously to study COPII proteins, including the *feelgood* (*creb3l2*; Melville *et al.*, 2011), and *crusher* (*sec23*; Lang *et al.*, 2006) mutants, but neither Ctage5 nor Tango1 has been investigated in this model system. In this study, we generated *ctage5* and *tango1l* mutant zebrafish and characterized phenotypes in the single- as well as double-homozygous mutant animals. We find that like other COPII pathway mutants, *ctage5* and *tango1* mutant zebrafish are small and have decreased survival. Overall, our studies reveal that Ctage5 and Tango1 have complementary, but also divergent roles in craniofacial development, collagen and lipoprotein trafficking, and in activation of cellular stress pathways.

## RESULTS

### Morphogenesis and survival are differentially affected by *ctage5* or *tango1l* deletion

To investigate how disruption of *ctage5* and *tango1* affects zebrafish development and survival, large portions of genomic coding sequence were deleted with Crispr/Cas9, eliminating critical functional domains (Figure 1A). At the *mia2* gene locus, transcripts of the *ctage5* mutant variant were decreased twofold compared with wild-type *ctage5* mRNA (Supplemental Figure S2). For the *mia3* gene locus, the deletion specifically eliminates the genomic region that transcribes and translates the unique luminal portion of *tango1l*, sparing the *tango1s* transcript. Primers designed to measure *tango1s* mRNA did not reveal a change between wild-type and *tango1l* mutant embryos, suggesting that Tango1s protein could still be made (Supplemental Figure S2). Furthermore, our analysis indicated there was no compensatory up-regulation of *ctage5* or *tango1* expression with deletion of the other gene (Supplemental Figure S2). Therefore, our study is designed to investigate deletion of *ctage5* or *tango1l (*subsequently referred to as *tango1).*

During embryogenesis, *ctage5* mutants look normal except for having darker yolk (Figure 1B). When raised at low rearing density (10 fish per tank), *ctage5* mutants are shorter (Figure 1C) and have decreased mass (Figure 1D) but can survive to expected numbers (Figure 1E). When raised at a high density (30 fish per tank), however, mutants have reduced survival (Supplemental Figure S3B). Regardless of rearing density, most *ctage5* mutants die by 1 year, while heterozygous and wild-type siblings show normal survival past 3 years. In contrast to *ctage5* mutant embryos, *tango1* mutants are significantly shorter, have obvious craniofacial defects, as the mouth fails to protrude past the eyes, and do not survive to adulthood regardless of rearing density (Figure 1, B and E; Figure S3A). The *ctage5;tango1* double mutants have similar, but more severe phenotypes compared with single mutants and also fail to survive to adulthood (Figure 1, B and E). Together, these results suggest that *ctage5* and *tango1* mutations differentially affect zebrafish during development and homeostasis, pointing to potential differences in cellular function.

### Craniofacial and other morphological defects in *tango1* mutants are accentuated with loss of *ctage5*

Mutations in COPII trafficking pathway components commonly cause craniofacial defects (Lang *et al.*, 2006; Townley *et al.*, 2008; Melville *et al.*, 2011). For example, in mice, loss of Tango1 causes dwarfed embryos with defects in cartilage formation and bone mineralization (Wilson *et al.*, 2011). Alcian blue staining confirmed that like mice, zebrafish *tango1* mutant embryos have defects in cartilage formation at 4dpf (Figure 2A). *ctage5;tango1* double mutants

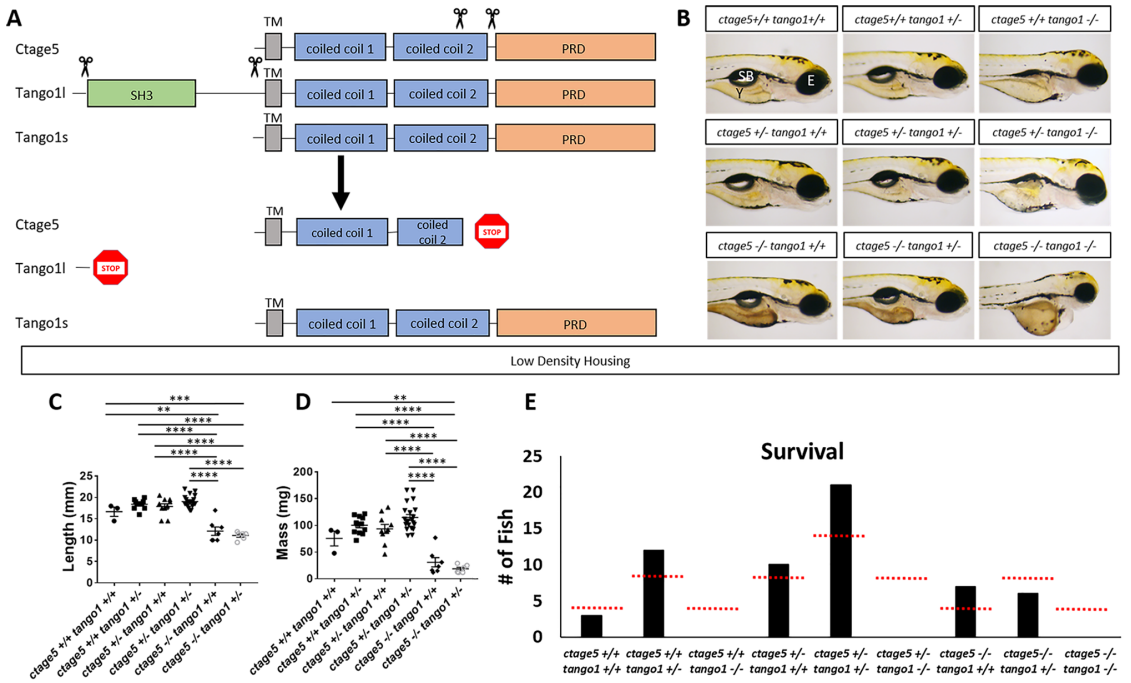


FIGURE 1: *ctage5* and *tango1* mutations affect size and survival of zebrafish: (A) Schematic showing CRISPR guide RNA cut sites (scissors) and the estimated final truncated proteins. (B) Representative brightfield images of all combinations of *ctage5* and *tango1* mutations in 4dpf zebrafish larvae. Y = yolk, SB = swim bladder, E = eye. (C) Length (one-way ANOVA, $F = 38.6$, $p < 0.0001$), (D) mass (one-way ANOVA, $F = 28.22$, $p < 0.0001$) and (E) survival ($\chi^2 = 24.59$, $p < 0.05$, $n = 59$) measurements of all combinations of *ctage5* and *tango1* mutant zebrafish at 2 mo raised in a low-density environment (about 10 fish per tank). Red-dotted lines in E represent expected survival, and black bars are actual survival. ** = $p < 0.01$, *** = $p < 0.001$, **** = $p < 0.0001$.

have a near-complete absence of cartilage staining (Figure 2A). Histology also revealed severe craniofacial defects in *tango1* mutant embryos that were exacerbated by *ctage5* deletion (Figure 2B). Interestingly, ocular lens defects exemplified by increased cell death and a degenerative lens were only observed in *ctage5;tango1* double mutant embryos (Figure 2, C and D). Although *ctage5* mutant lenses appear normal during development, by 2 months lens epithelial defects were observed (Figure 2E), suggesting a lens homeostasis role for Ctage5. Cardiac chamber dysgenesis was another unique phenotype to *ctage5;tango1* double mutants. While both *ctage5* and *tango1* mutants showed normal heart development, severe cardiac structural changes were apparent by 4dpf when these genes were disrupted in tandem (Figure 2F). However, blood pooling in the caudal vein was noticed in both *tango1* single and *ctage5;tango1* double mutant larvae, suggesting that *tango1* mutation could be driving cardiovascular defects, which only become obvious with the additional deletion of *ctage5* (Figure 2G). These results extend previous in vivo observations demonstrating that Tango1 plays a critical role in morphogenesis of multiple tissues. However, Ctage5 also acts in many developmental processes, as phenotypes observed in *tango1* mutants are enhanced by *ctage5* deletion.

### Large-molecule trafficking defects differ between *ctage5* and *tango1* mutants

TANGO1 has been well established as a cargo receptor for collagen trafficking in various cell types in vitro and in vivo (Saito *et al.*, 2009; Wilson *et al.*, 2011; Maeda *et al.*, 2016; Maiers *et al.*, 2016; Gorur *et al.*, 2017; Rios-Barrera *et al.*, 2017). CTAGE5 is necessary for collagen VII trafficking in an epidermal carcinoma human cell line (Saito *et al.*, 2011), but its role in secreting other collagens and in other cell lines or in vivo is still largely unknown. Lipoprotein trafficking is also altered with loss of CTAGE5 or TANGO1 (Santos *et al.*, 2016; Wang *et al.*, 2016; Zhang *et al.*, 2018). To begin investigating large-molecule trafficking in zebrafish, we performed wholemount staining for Collagen II. The branchial arch cartilage of wild-type and *ctage5* mutant animals showed extracellular Collagen II surrounding chondrocytes. In contrast, in *tango1* and double mutants, Collagen II was found in intracellular puncta within chondrocytes (Figure 3A). With decreased trafficking of large molecules, we hypothesized that protein buildup occurred within the ER, which would be consistent with previous reports of distended ER after loss of Tango1 (Wilson *et al.*, 2011; Petley-Ragan *et al.*, 2016; Rios-Barrera *et al.*, 2017; Maiers *et al.*, 2016). Indeed, we observed distended ER in *tango1* and double mutant chondrocytes, while the ER in *ctage5* mutants and wild-type chondrocytes was normal (Figure 3B). We next investigated lipoprotein trafficking using a lipid analog, BODIPY-c12, that has previously been shown to require β-lipoproteins for trafficking from the yolk into the zebrafish vasculature (Miyares *et al.*, 2014). Efficient β-lipoprotein trafficking was observed in wild-type larvae by monitoring BODIPY-c12 vascular fluorescence following injection into the yolk. However, BODIPY-c12 trafficking was decreased in *tango1* mutants, and nearly undetectable in *ctage5* or double mutant embryos (Figure 3C). Oil Red O staining confirmed this significant loss of serum lipids in *ctage5* single and *ctage5;tango1* double mutant embryos (Figure 3D). Together these results suggest that lipoprotein trafficking is significantly affected after deletion of Ctage5, and to a lesser extent with loss of Tango1, consistent with results reported from the Malhotra Lab (Santos *et al.* 2016). Conversely, in cell types that secrete large amounts of collagen, such as chondrocytes, deletion of *tango1*, but not *ctage5* severely affected protein export and ER maintenance.

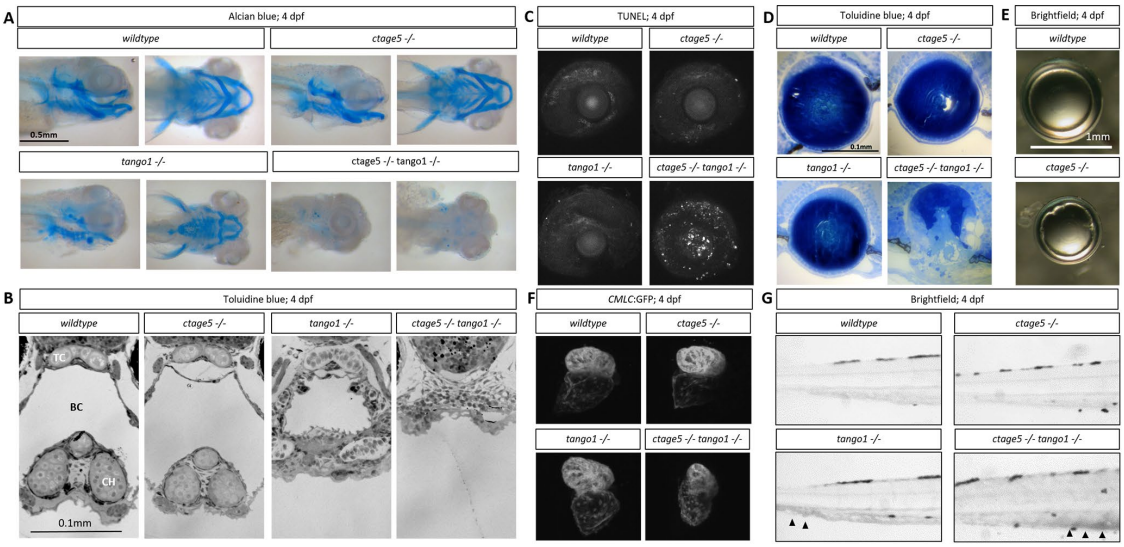


FIGURE 2: Craniofacial and other morphological defects in *tango1* mutants are accentuated by *ctage5* deletion. (A) Representative lateral (left) and ventral (right) images of Alcian blue–stained 4dpf larvae. (B) Representative images of plastic-sectioned and toluidine blue–stained 4dpf larvae cropped to show craniofacial alterations. TC = trabeculae, BC = buccal cavity, CH = ceratohyal cartilage. (C) Representative maximum intensity projection images showing TUNEL staining of 4dpf lens and sclera. (D) Representative images of plastic-sectioned and toluidine blue–stained 4dpf lens. (E) Representative images of lens dissected from 3-mo-old zebrafish. (F) Representative images showing ventricle-enriched cardiac myosin light chain (*CMLC*:GFP) expression. (G) Representative brightfield image of the trunk for each genotype. Arrowheads detail blood pooling in the caudal vein.

### Cell stress is differentially activated in tissues after *ctage5* or *tango1* deletion

When cellular trafficking is affected and cargo builds up at the ER, the evolutionarily conserved unfolded protein response (UPR) can be activated (Walter and Ron, 2011). Numerous reports suggest ER stress and autophagy can be altered after deletion of *CTAGE5* or *TANGO1* (Wilson *et al.*, 2011; Maiers *et al.*, 2016; Petley-Ragan *et al.*, 2016; Santos *et al.*, 2016; Fan *et al.*, 2017; Ge *et al.*, 2017; Rios-Barrerra *et al.*, 2017), but a direct comparison of either factor on the ATF6 ER stress or autophagy has not been carried out. We recently described a transgenic zebrafish line to measure the ATF6 activation, which mediates the major transcriptional response to ER stress (Clark *et al.*, 2020). Using these transgenic fish, we observed that *ctage5*-/-; *tango1*-/- larvae have significantly increased *ATF6* reporter fluorescence in the spinal cord at 4dpf (Figure 4, A and A'). As assessed by nuclei packing and cell body morphology, spinal cord cells in the double mutants are disorganized and in some instances mislocalized from the normal lamination pattern (Figure 4, B and B', asterisk). Although spinal cord cells of *ctage5* single mutants were unaffected at 4dpf, by 7dpf these larvae had significantly increased *ATF6* reporter activation (Figure 4, C and C'). Furthermore, 7dpf *ctage5* mutant larvae had increased lysosomal volume in the spinal cord and brain compared with wild-type or *tango1* mutants (Figure 4, D, D', E, and E'). In addition, within the brain, *ctage5*;*tango1* double mutant embryos showed significant increase in cell death markers, while single mutations were similar to wild-type brains (Figure 4, F and F'). As adults, *ctage5* mutant zebrafish show elevated *gap43*:GFP expression (Figure 4G). Expression of *gap43* is known to be induced with neuronal stress (Skene, 1989; Benowitz and Routtenberg, 1997; Bormann *et al.*, 1998; Kaneda *et al.*, 2008; Udvadia 2008; Diekmann *et al.*, 2015). Therefore, *ctage5* mutant larvae undergo cellular stress throughout the nervous system, as evidenced by activated ER stress, altered cell morphology, and elevated autophagy and apoptosis, which continue into adulthood. Our observations are consistent with the axonal trafficking defects described in mice with conditional *Ctage*5 deletion from the nervous system (Zhang *et al.*, 2018). We also noticed ER stress in other tissues including the jaw in *tango1* mutant and double mutant larvae, but not in *ctage5* mutant embryos, consistent with craniofacial defects observed in Figure 2 (Figure 5, A, A', B, and B'). Conversely, ER stress was observed in the intestine of *ctage5* mutant larvae but not *tango1* mutants at 7dpf (Figure 5, C and C'). Within trunk skeletal muscle, both *ctage5* and *tango1* mutant embryos showed ATF6-ER stress (Figure 5, D, D', E, and E'). Interestingly, however, *ctage5* mutants show significantly elevated *ATF6* activation in the muscle fibers, whereas in *tango1* mutants the ER stress is activated along cells lining the chevron-shaped muscle segments. The role for Ctage5 or Tango1 in muscle tissue has not been investigated previously, but these data suggest that Ctage5/Tango1 family of proteins also have divergent functions in that tissue type.

## DISCUSSION

CTAGE5 and TANGO1 are both known to act in the COPII trafficking pathway (Saito *et al.*, 2009, 2011), but until now the effects of deleting these proteins in the same model system have not been investigated. Our results suggest that zebrafish Ctage5 and Tango1 have complementary, but also divergent roles across multiple tissues (Figure 6). For example, we found that both factors affect fish growth when deleted. *tango1* mutant fish are shorter at larval stages, whereas *ctage5* mutant larvae are morphologically normal initially, but those that survive are much smaller than their wild-type siblings. Consistent with our results, global knockout of *Tango1* inhibits growth in mouse embryos (Wilson *et al.*, 2011). Interestingly, conditional knockout of *Ctage5* in the mouse brain or liver also results in decreased animal size (Wang *et al.*, 2016; Zhang *et al.*, 2018), indicating that Ctage5 function in multiple organ systems is important for embryonic growth and development.

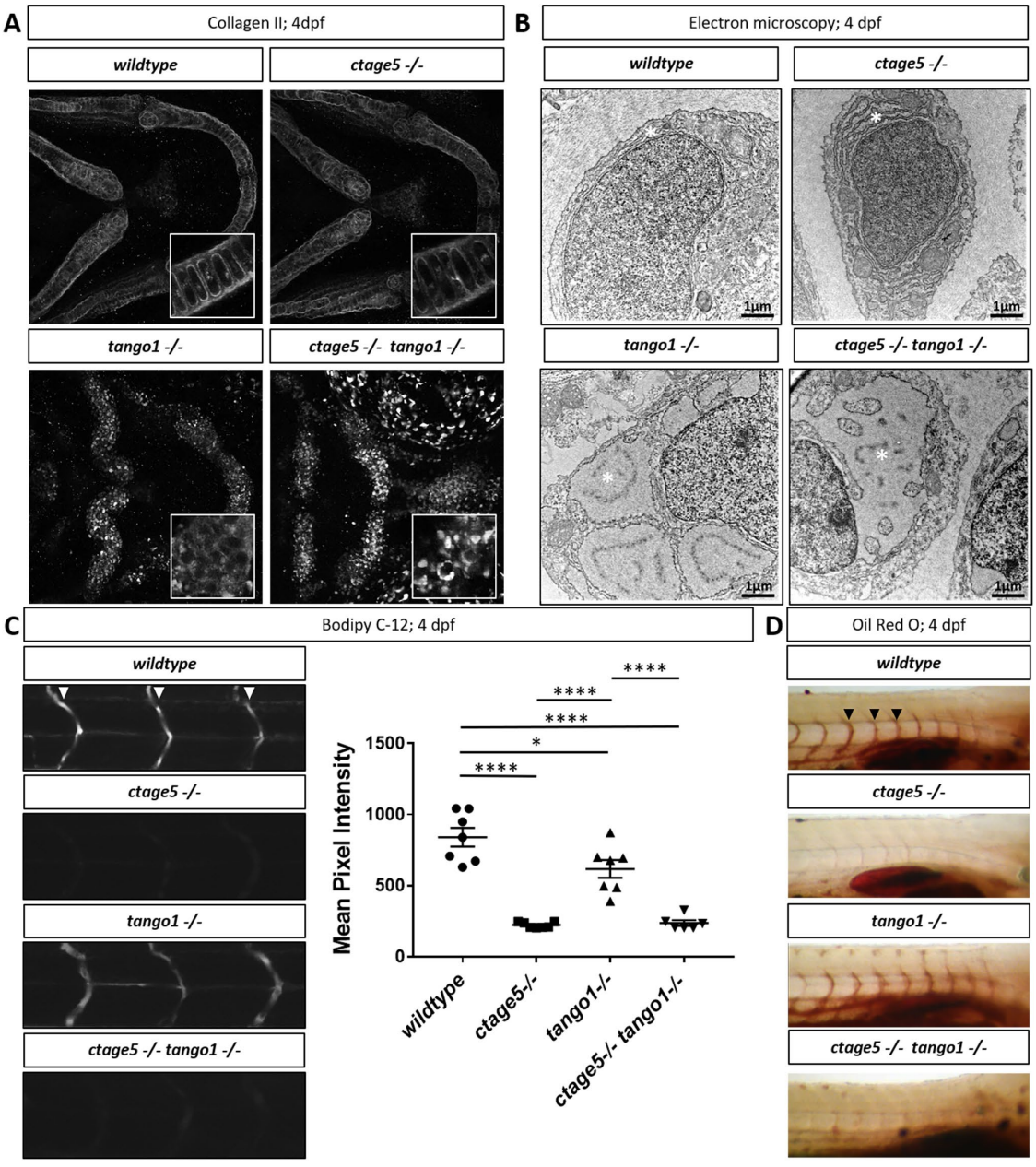


**FIGURE 3:** Trafficking differences in *ctage5* vs. *tango1* mutant embryos. (A) Representative 40× images showing collagen 2 wholemount immunohistochemistry in 4dpf larvae chondrocytes ($n = 3$–4 per group). Inserts are 40× images with 3× zoom and cropped to show higher-resolution chondrocyte collagen 2 staining. (B) Representative electron microscopy images of endoplasmic reticulum (*) in 4dpf larvae chondrocytes ($n = 3$ per group). (C) Representative images and quantification of BODIPY C-12 fluorescence in the intersegmental vessels (arrowheads; one-way ANOVA, $F = 39.36$, $p < 0.0001$). (D) Representative images of Oil Red O staining for lipids in 4dpf zebrafish larvae intersegmental vessels (arrowheads). * = $p < 0.05$, **** = $p < 0.0001$.

More striking differences in *tango1* versus *ctage5* mutant phenotypes were characterized for collagen secretion. Collagen II export was blocked in *tango1* mutant larvae, most notably in the chondrocytes, resulting in distended ER and craniofacial defects. *ctage5* mutants, however, have normal collagen II trafficking in chondrocytes and craniofacial structures appeared normal. These results are in line with findings from Wilson *et al.* (2011), where trafficking of multiple collagens were affected with loss of TANGO1 resulting in severe craniofacial defects. In our study, we found similar results by investigating Collagen II trafficking. Prior to our study, the role of CTAGE5 in collagen trafficking in vivo had not been investigated. In vitro studies, however, showed that collagen VII trafficking is disrupted by deletion of *CTAGE5* (Saito *et al.*, 2011). Our results suggest that collagen II trafficking is not affected with *ctage5* deletion alone, indicating that Tango1 has a more significant role in Collagen II trafficking and craniofacial development.

In contrast to collagen trafficking, lipoprotein trafficking was predominantly affected by mutation to *ctage5*, where lipoprotein trafficking from the yolk into the zebrafish embryo was completely disrupted. Previous studies have shown that lipoprotein trafficking and lipid profiles are altered with loss of CTAGE5 or TALI (Wang *et al.*, 2016; Santos *et al.*, 2016, Zhang *et al.*, 2018). Our results are

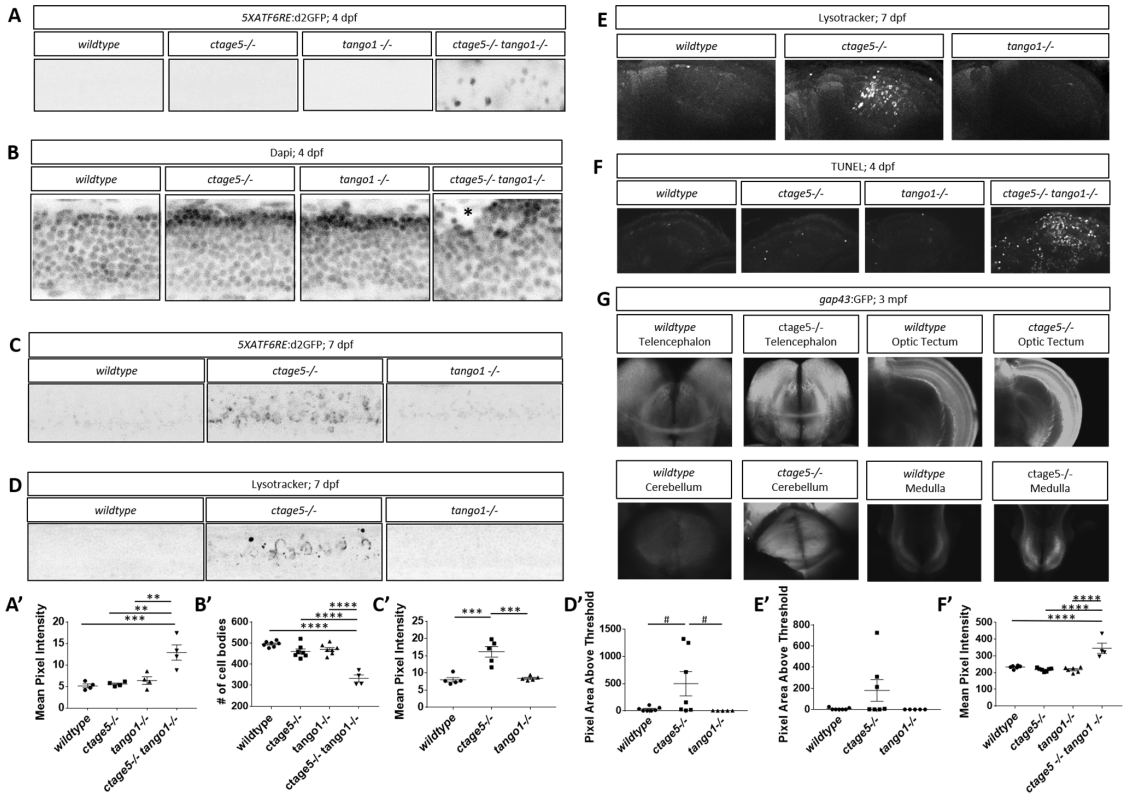


**FIGURE 4:** Stress pathway activation in the nervous system is specific for *ctage5* -/- and amplified by *tango* mutation. (A, A′) Representative images, A, and quantification, A′, of *5XATF6RE*:d2GFP activation in 4dpf spinal cords (one-way ANOVA, $F = 12.42$, $p = 0.0005$). (B, B′) Representative images of DAPI staining, B, and quantification of brightfield images, B′, in 4dpf spinal cords to show cellular organization (asterisk shows cells mislocalized from the normal lamination pattern; one-way ANOVA, $F = 37.51$, $p < 0.0001$). (C, C′) Representative images, C, and quantification, C′, of *5XATF6RE*:d2GFP activation in 7dpf spinal cords (one-way ANOVA, $F = 22.22$, $p < 0.0001$). (D, D′) Representative images, D, and quantification, D′, of the lysotracker staining area above threshold for acidic compartments in 7dpf spinal cords (one-way ANOVA, $F = 3.881$, $p = 0.0423$). (E, E′) Representative images, E, and quantification, E′, of the lysotracker staining area above threshold of lysotracker for acidic compartments in 7dpf brains (one-way ANOVA, $F = 2.479$, $p = 0.1154$). (F, F′) Representative images, F, and quantification, F′, of TUNEL staining for cell death in 4dpf brains (one-way ANOVA, $F = 24.33$, $p < 0.0001$). (G) Representative images of *gap43*:GFP in 3–mo old PACT cleared *ctage5* wildtype (WT) or homozygous mutant brains. $^{\#} = p < 0.08$, ** = $p < 0.01$, *** = $p < 0.001$, **** = $p < 0.0001$.

consistent with these studies and extend these findings through a direct comparison of Ctage5 and Tango1 for lipid trafficking in vivo. These results suggest that Tango1 plays a primary role in collagen trafficking, whereas Ctage5 is more important for lipoprotein trafficking.

While our studies addressed the shared and unique functions between Ctage5 and Tango1 with respect to trafficking and cellular homeostasis, the experiments in zebrafish also demonstrated that Tango1 plays an important role in maintaining ER-Golgi morphology, consistent with observations by others (Bard *et al.*, 2006; Liu *et al.*, 2017; Rios-Barrerra *et al.*, 2017; Reynolds *et al.*, 2019). CTAGE5 also remodels ER-exit sites and plays a role in the ER and ER Golgi intermediate compartment (ERGIC), creating an autophagy supply pathway (Ge *et al.*, 2017). In this regard, our observation of increased lysosomal volume in *ctage5* mutants is consistent with compensatory up-regulation of lysosome-mediated protein degradation. As lysosomal volume was unchanged in *tango1* mutants, these data suggest a specific role of Ctage5 in autophagosome formation. Overall, our data confirm and extend the important, but surprisingly divergent and cell type–specific roles of Ctage5 and Tango1 in large–cargo trafficking and intracellular membrane dynamics.

In our experiments, there were some limitations on separating complementary and divergent functions from tissue and cellular expression differences. In mouse and human studies, Tango1 and Ctage5 are expressed ubiquitously (Maeda *et al.*, 2016; Santos *et al.*, 2016). Bulk tissue RNAseq (Askary *et al.*, 2017; White *et al.*, 2017; Burkhard and Bakkers, 2018; San *et al.*, 2018) and the scRNA seq EMBL-EBL atlas also suggest ubiquitous expression, but that different cell types within a tissue could have different expression levels of *ctage5* and *tango1*. The cell-type differences in expression levels could be coupled to cellular trafficking demand, potentially explaining some of the differences in phenotypes with loss of either ctage5 or tango1. Zebrafish also receive maternal (wild-type) proteins from the yolk, which can complicate loss-of-function phenotypes in embryos derived from heterozygous incrosses. However, yolk trafficking defects observed in the mutants indicate maternal protein rescue is not a significant confound. Finally, it is possible that Tango1s protein is generated in the *tango1* mutant used for analysis (Supplemental Figure S1). In future studies, it will be interesting to address potential functional redundancy and differences in Tango1l versus Tango1s.

With the described results and limitations in mind, there are a couple of hypotheses for complementary and divergent functions at

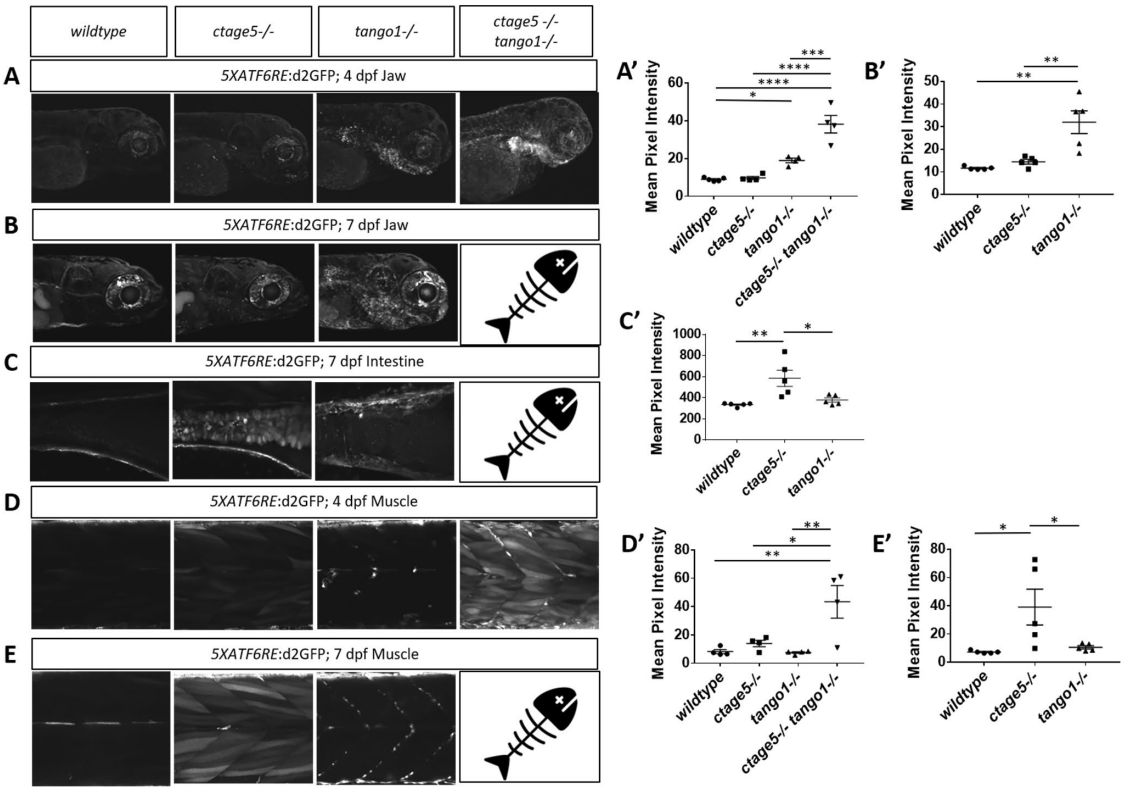


FIGURE 5: ER stress is prevalent in tissues outside of the nervous system. Representative images and quantification of 5XATF6RE:d2GFP ER stress in the jaw at 4dpf (A, A'; one-way ANOVA, $F = 34.44$, $p < 0.0001$) and 7dpf (B, B'; one-way ANOVA, $F = 13.86$, $p < 0.0008$), intestine at 7dpf (C, C'; one-way ANOVA, $F = 8.358$, $p = 0.0053$), and muscle at 4dpf (D, D'; one-way ANOVA, $F = 8.205$, $p = 0.0031$) and 7dpf (E, E': $F = 5.624$, $p = 0.0189$). * = $p < 0.05$, ** = $p < 0.01$, *** = $p < 0.001$, **** = $p < 0.0001$. = indicates *ctage5-/- tango1-/-* mutants do not survive to 7dpf.

the ER: 1) *Expression-based explanation*: Some cell types express more *ctage5* or *tango1*, and so different proportions of protein are localized at the ER. Loss of the predominant protein would have the largest effect on the cell type, while loss of the minor abundant protein may have a smaller effect. 2) *Function-based explanation*: 2A) *ER subdomains*: Even if *ctage5* and *tango1* are expressed at similar levels, one protein could predominate at ERESs or subdomains within an ERES (Maeda *et al*., 2019). ER domains that are more concentrated with either Ctage5 or Tango1 could be related to the primary molecule being secreted from that domain. Deletion of one factor could cause a specific effect through elimination from the subdomain, but residual activity could persist until the other factor is deleted causing a complementary effect. 2B) *ERES interactions*: Ctage5 and Tango1 could always be located in the same ERES but interact in different homo- and heterodimers, resulting in divergent functions. Therefore, deletion of one component could eliminate a subset of interactions and lead to specific trafficking defects. Deletion of an additional factor would eliminate more complexes at the ERES causing a complementary effect. Aside from interactions within the family, CTAGE5 and TANGO1 have unique interactions with many other protein families (Stark *et al*., 2006), further supporting specific cellular functions. Investigating expression coupled with specific interactions and ERES subdomain localization in the cell types that were described in this study will be an interesting to pursue with future experimentation.

Several observations from our studies have relevance to human disease. The nervous system was severely affected by *ctage5* deletion, consistent with descriptions in mice (Zhang *et al*., 2018). We found neuronal stress was not observed with deletion of *tango1* alone, but *ctage5* mutant–dependent stress was exacerbated with *tango1* deletion. Interestingly, in humans, the CTAGE5 variant P521A was identified as a risk factor for Fahr's disease, a rare neurologic disorder (Oliveira *et al*., 2007; Lemos *et al*., 2011). Furthermore, by investigating organ systems not previously characterized, we discovered that *tango1* and *ctage5* mutant cells in the intestine, muscle, and heart show elevated ER stress and morphological abnormalities. Cardiac defects in *tango1* mutants are particularly interesting as the European Biomedical Institute GWAS catalogue reports that multiple heart diseases, including coronary artery disease, coronary heart disease, and myocardial infarction, are associated with *TANGO1* intron variants (Buniello *et al*., 2019). Very recently, homozygous hypomorphic coding mutations in human *TANGO1* were shown to result in collagen secretion defects leading to short stature and skeletal and neuronal defects, as well as insulin-dependent diabetes (Lekszas *et al*., 2020). Establishing the role of Ctage5 and Tango1 in multiple cellular processes and specific cell types in zebrafish suggests that this model system will be valuable to assess other candidate disease variants in human *CTAGE5* and *TANGO1*.

In conclusion, our study uses the zebrafish model system to define the in vivo consequences when the cellular functions of cTAGE5 and TANGO1 are disrupted. Through this analysis, complementary and divergent roles for these proteins have been discovered, including identification of novel physiological processes and tissue dependences on these factors.

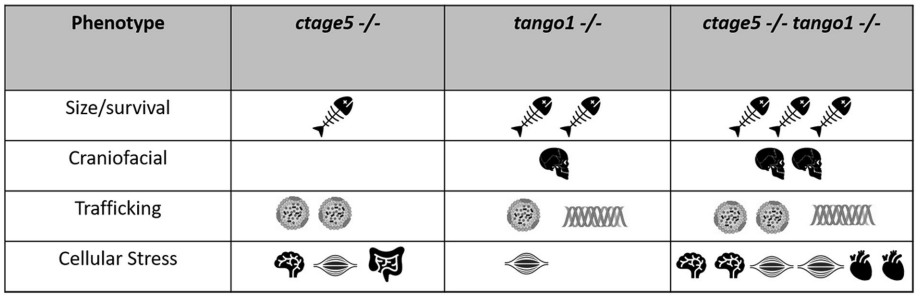


FIGURE 6: Summary of phenotype magnitude in mutant fish. Table summarizing phenotype severity. Any symbol represents an elevated severity compared with *wild-type*. More symbols represent increased severity. Survival/size defects, craniofacial defects, lipoprotein, collagen, brain, muscle, intestine, heart.

## MATERIALS AND METHODS

Request a protocol through *Bio-protocol*.

### Mutant generation

Clustered regularly interspaced short palindromic repeats (CRISPR) guides were designed using ZiFiT Targeter Version 4.2 (http://zifit.partners.org/ZiFiT, in the public domain) against regions of zebrafish *ctage5* exon14, 5′-GGCCGCAAGGGCAGCTGATC-3′, and exon18 5′-GGCCTCCTATATGGCAAACC-3′ (ensemble transcript mia2-205). CRISPR guides targeting *tango1* were designed against exon1, 5′-TGGCTGCACCGAATAATCCC-3′, and exon7, 5′-ATCTGAAGTCGATGAGTCGG-3′ (ensemble transcript mia3-202). CRISPR gRNA templates were generated by cloning annealed oligonucleotides with appropriate overhangs into BsaI-digested pDR274 plasmid. CRISPR gRNAs were synthesized using a MEGAshortscript T7 Transcription Kit and purified using a mirVana miRNA Isolation Kit (Ambion, Austin, TX, USA). Zebrafish codon-optimized cas9 was synthesized using a mMESSAGE mMACHINE Kit (Ambion) and polyadenylated using a Poly(A) Tailing Kit (Ambion). CRISPR gRNAs and cas9 mRNA were coinjected into one- to four-cell zebrafish embryos from wild-type ZDR fish maintained internally in the Link lab at 10 and 50 ng/μl, respectively, and surviving embryos were raised to adulthood before outcrossing to identify the founder fish carrying germline edits in *ctage5* or *tango1*. Offspring from these fish were raised to adulthood and then fin-clipped for genotyping (see below for details). The resulting 6285-bp deletion *ctage5* mutant and 14,043-bp deletion *tango1* mutant described here were identified via sequencing (Retrogen, San Diego, California, USA).

Mutant and transgenic fish used for experiments:

*ctage5* mutant: *mia2*$^{mw91}$ (this study)

*tango1l* mutant: *mia3*$^{mw92}$ (this study)

Tg(Tru.Gap43:EGFP) (Udvadia 2008)

Tg(Hsa.ATF6RE-fasab:d2eGFP)$^{mw85Tg}$ (Clark *et al.*, 2020)

### Genotyping

Genomic DNA was extracted from zebrafish tissue using a Puregene Core Kit (Qiagen, Hilden, Germany). The genomic region containing either the *ctage5* or *tango1* mutation was amplified by PCR. The PCR protocol utilized primers flanking the expected deletion to identify the mutant allele and one primer flanking the expected deletion and one inside the deleted region to identify the wildtype allele.

To identify the *ctage5* wildtype allele, a forward primer for exon 13, 5′-AAGGCTCATGATAACTGG-3′, and a reverse primer for exon 14, 5′-GAGCGTTTTCTCTC-TTGA-3′, creating a 171-bp amplicon. For the *ctage5* mutant allele, the exon 13 forward primer was paired with a reverse primer for exon 18, 5′-AGGAAGTGGAG-GTCTAGG-3′, creating a 204-bp amplicon. To identify the *tango1* wildtype allele, a forward primer for exon 1, 5′-TGTTGGT-GCTGCTATCTC-3′, and a reverse primer for exon 1, 5′-CTGCTGCATTCTTCAT-CCG-3′ were used to generate a 262-bp amplicon. For the *tango1* mutant allele, the exon1 forward primer was paired with a reverse primer for exon 7, 5′-GTAGTACT-CACAATCTCTCC-3′, creating a 237-bp amplicon.

### Fish maintenance

Zebrafish (*Danio rerio*) were maintained at 28.5°C in an Aquatic Habitats recirculating filtered water system (Aquatic Habitats, Apopka, FL) in reverse-osmosis purified water supplemented with Instant Ocean salts (60 mg/l) on a 14-h light:10-h dark lighting cycle and fed a standard diet (Westerfield, 1995). All animal husbandry and experiments were approved and conducted in accordance with the guidelines set forth by the Institutional Animal Care and Use Committee of the Medical College of Wisconsin.

### Survival analysis and size measurements

Zebrafish embryos were added to the Aquatic Habitats system at 5dpf at either high density (30 embryos per tank) or low density (10 embryos per tank). At 2 months, zebrafish were anesthetized in Tricaine and blotted with paper towels, mass length was calculated, and fin clips were collected. gDNA was extracted from the fin clips and genotyped.

### Plastic sectioning and electron microscopy

4dpf embryos were fixed in cacodylate fix (0.1M cacodylate, 2% PFA, 2% glutaraldehyde [pH 7.4]) at 4°C overnight, postfixed in 1% osmium buffer solution, dehydrated through a series of methanol and acetonitrile washes, and infiltrated with Embed 812 resin (14120; Electron Microscopy Sciences, Hatfield, PA). Semithin transverse sections (1 μm) were cut with glass knives on a Leica RM2255 microtome, heat-fixed to glass slides, stained with 1% toluidine blue in 1% borax buffer, and imaged on a Nikon Eclipse E800 light microscope with an attached Sony DSC HX1 camera to capture craniofacial images. Plastic blocks were then submitted to the Electron Microscopy Facility at the Medical College of Wisconsin for electron microscopy. Ultrathin sections (70–80 nm) were collected using a DiATOME Ultra 45° diamond knife (MT7376; DiATOME), collected on copper hexagonal mesh coated grids (G200H-Cu; Electron Microscopy Sciences), and stained with uranyl acetate and lead citrate for contrast. Images were captured using a Hitachi H600 TEM microscope (Hitachi, Tokyo, Japan).

### TUNEL

4dpf zebrafish embryos were fixed with 4% PFA overnight at 4°C. Fixed embryos were washed three times in phosphate-buffered saline (PBS) for 10 min, rinsed with dH20, and incubated with dH20 for 30 min at room temperature followed by acetone at –20°C for 30 min and 30 min dH20 to permeabilize embryos. Further, embryos were washed three times with PBST (PBS + 1% TritonX-100) and then incubated in 1 mg/ml Collagenase II in PBST for 90 min at

room temperature. Embryos were washed three times for 15 min in PBST and TUNEL reaction mixture (Roche), or the label solution alone was added for 2 h at 37°C as a control. Embryos were washed 3 × 15 min in PBS and then imaged using confocal microscopy. Mean pixel intensity was measured using ImageJ (Rasband, W.S. ImageJ, U.S. National Institutes of Health, MD), and quantified using GraphPad Prism software (GraphPad, La Jolla, CA).

### Alcian blue

Alcian blue cartilage staining was performed similarly to Hendee *et al.* (2018). 4dpf zebrafish embryos were fixed in 4% PFA overnight at 4°C. Fixed embryos were washed two times with 1× PBS for 5 min and bleached in 1 ml 10% hydrogen peroxide ($H_2O_2$) in ddH2O supplemented with 50 µl of 2M KOH for 1 h at room temperature with rotation. Embryos were stained with 0.1% Alcian blue solution composed of Alcian blue 8GX (Sigma-Aldrich, St. Louis, MO) dissolved in acidic ethanol. Stained embryos were briefly rinsed with acidic ethanol and then washed 4 × 60 min with acidic ethanol. Following washes, embryos were digested in 10 µg/mL proteinase K diluted in PBST (PBS + 0.1% Tween20) for 1 h at room temperature, refixed in 4% PFA, progressively dehydrated with ethanol, and stored in 80% glycerol. Wholemount images were obtained on a Leica MZFLIII dissecting scope with an attached Nikon E995 camera.

### Lysotracker red

7dpf zebrafish were treated with 10 µM LysoTracker (LysoTracker Red DND-99; L7528) in 1-phenyl 2-thiourea (PTU) or 1% DMSO in PTU for control embryos for 1 h at 28.5°C. Embryos were washed 3 × 15 min with PTU and then fixed with 4% PFA and imaged using confocal microscopy. Using ImageJ, a threshold was set to identify only high lysotracker staining, and the area was measured. Data were processed using Microsoft Excel (Microsoft, Redmond, WA) and graphed using GraphPad Prism (GraphPad, La Jolla, CA).

### Oil Red O

4dpf larvae were fixed with 4% PFA overnight at 4°C. Larvae were washed three times with PBS, rinsed with 60% isopropanol, and then incubated in 60% isopropanol for 30 min on a rotator at room temperature. Next, larvae were dyed in fresh filtered 0.3% Oil Red O in 60% isopropanol for 3 h and then washed multiple times with 60% isopropanol and dH20 until the nonspecific staining was removed. Washed larvae were mounted in agarose and imaged on a Leica MZFLIII dissecting scope with an attached Nikon E995 camera.

### Immunofluorescence

4dpf larvae were fixed overnight with 4% PFA at 4°C. For notochord staining, larvae were left intact, but for chondrocyte staining, trunks were removed and used for DAPI staining and only the head was stained. Antigen retrieval was used for chondrocyte staining by incubating larvae in antigen retrieval buffer (150 mM Tris-HCL, pH 9), followed by heating to 70°C in antigen retrieval buffer for 15 min, and washed two times for 10 min in PBST (0.1–1% Triton in PBS) at room temperature. All following steps were completed on a rotator when possible. Larvae were permeabilized by washing once with $dH_20$ followed by $dH_20$ for 30 min at room temperature, acetone for –20°C for 30 min, $dH_20$ for 30 min, and 10 µg/ml proteinase K in PBST at room temperature. Then 4% PFA was added for 20 min at room temperature to postfix and washed three times for 15 min in PBST. Larvae were incubated in PBDT buffer (1% DMSO, 1% BSA, 0.5–1% Triton X-100, 1× PBS) with 5% goat serum (NGS) for 60 min at room temperature. Collagen II (II-II6B3; 1:100; Developmental Studies Hybridoma Bank) was stained overnight in the chondrocytes in PBDT/5% NGS at 4°C. Larvae were washed with PBST six times for 15 min at room temperature and then incubated with secondary antibody (1:400) in 2% NGS/PBDT for 4 h at room temperature. Larvae were washed six times with PBST for 15–20 min, and if necessary, were stained with DAPI (1:1000 in PBST) for 30 min at room temperature and washed three times in PBS. Larvae were then mounted and imaged using confocal microscopy.

### Adult lens dissection

Three-month-old zebrafish were fixed overnight with 2% PFA at 4°C. Zebrafish lenses were dissected from the eye globe and imaged using a Leica MZFLIII dissecting scope with an attached Nikon E995 camera.

### Labeled fatty acid injection into yolk

To analyze lipid transport from the zebrafish embryo yolk into the body, fluorescently tagged BODIPY (BODIPY FL $C_{12}$; Invitrogen D3822) stock was dried completely in a speed vacuum and resuspended in canola oil to a final concentration of 1 mg/ml. The BODIPY oil mixture (4.6 nl) was injected into the zebrafish yolk at 4dpf. Four hours after injection, zebrafish intersegmental vessels in the trunk were imaged using confocal microscopy. For measuring the mean pixel intensity of BODIPY- $C_{12}$ in the intersegmental vessels, three vessels were averaged as a single data point using Microsoft Excel (Microsoft, Redmond, WA) and graphed using GraphPad Prism (GraphPad, La Jolla, CA).

### RNA extraction and real-time PCR

Analysis of *ctage5 and tango1* transcripts was performed on whole embryos. mRNA was extracted from dechorionated embryos at 7dpf using TRizol–chloroform treatment. The isolated aqueous phase from the resulting TRizol–chloroform gradient is transferred to a new tube and incubated with isopropanol at room temperature for 10 min. Centrifugation at 4°C for 10 min results in formation of an RNA pellet, which is then washed with 75% ethanol in diethyl procarbonate (DEPC)-treated water. Following this wash, the pellet is allowed to dry and is resuspended in DEPC-treated water with a 10-min incubation at 60°C. Resuspended RNA is then subjected to a DNAse treatment and concentration is quantified.

cDNA was generated using the Superscript III First-Strand Synthesis System for RT-PCR Kit (Invitrogen) per manufacturer's instructions, and all qRT-PCR was performed on a CFX Connect Real-Time System (Bio-Rad) using PrimeTime Gene Expression Master Mix (IDT). qRT-PCR was performed on five biological replicates, and all biological replicates were run in triplicate for each transcript. The zebrafish housekeeping gene *ef1a* was used for normalization. Statistical significance of differences in transcript abundance was calculated using Welch's *t* test. qPCR sequences are as follows:

*ctage5* exon 7–9:

Primer 1: CTCATCTTGGCCGCTTCTAT

Primer 2: CATCGACGGCAGCACTAATA

*ctage5* exon 19–20:

Primer 1: GGCGGAGGCATTGACATTA

Primer 2: AGAGAAGGCTCTGGAGATATGA

*tango1* exon 28–29:

Primer 1: AGAGGTCCAGGCGGAAA

Primer 2: CACACATCGGCCCGTTT

### Imaging and data analysis

Fluorescence was detected using Nikon Eclipse E600FN or C2 Nikon Eclipse 80i confocal systems. Mean pixel intensity was measured using ImageJ (Rasband, W.S. ImageJ, U.S. National Institutes of Health, MD). To measure spinal cord cell number, spot detection software was used in Imaris (Bitplane, Zurich, Switzerland). For survival analysis, a $\chi^2$ analysis was performed with the expected numbers calculated from the total number of fish collected at the 2-mo timepoint when fish were genotyped and counted. Data were processed using Microsoft Excel (Microsoft, Redmond, WA) and graphed using GraphPad Prism (GraphPad, La Jolla, CA). An unpaired two-tailed *t* test was used to analyze graphs with two groups. For three or more groups, a one-way ANOVA was conducted with Tukey's post hoc analysis for pairwise comparisons.

### Adult brain clearing

PACT clearing was performed based on Cronan *et al.* (2015) with slight modifications. Briefly, zebrafish were fixed in 2% paraformaldehyde (PFA) for 1 day at 4°C. The fixed whole adult fish brain was dissected and incubated at 4°C for 1 day in ice-cold, freshly made hydrogel monomer solution of A4P0 (4% acrylamide in PBS) supplemented with 0.25% VA-044. A4P0-infused samples were incubated for 3 h at 37°C to initiate tissue-hydrogel hybridization. Hydrogel monomer solution was removed and washed three times with PBS. Whole brains were then incubated in 8% SDS in 200 mM boric acid, pH 8.5, at 37°C under shaking for 5 h or until the brain periphery was clear. This solution was replaced with PBST and samples were left to shake overnight at room temperature, allowing the center of the brain to clear overnight. Samples were then washed throughout the day with four changes of PBS, 0.1% Triton X-100 at room temperature, and then incubated overnight in RIMS imaging media (Yang *et al.*, 2014) at room temperature on a rotator. Samples were stored in RIMS at room temperature until imaged using confocal microscopy.

## ACKNOWLEDGMENTS

The authors thank Michael Cliff, William Hudzinski, and Edi Kuhn for zebrafish husbandry, Jon Bostrom for help with CRISPR design, and Elena Semina and her laboratory for assistance with Alcian blue staining. We are also grateful to Clive Wells for help with electron microscopy experiments. This work was supported by the National Institutes of Health/National Aging Institute (R21AG066038 to B.A.L.), the Clinical and Translational Science Institute, Medical College of Wisconsin (TL1TR001437 Award to E.M.C.), and the Foundation Fighting Blindness (PPA-0617-0718).

## REFERENCES

Askary A, Xu P, Barske L, Bay M, Bump P, Balczerski B, Bonaguidi MA, Crump JG (2017). Genome-wide analysis of facial skeletal regionalization in zebrafish. Development 144, 2994–3005.

Bard F, Casano L, Mallabiabarrena A, Wallace E, Saito K, Kitayama H, Guizzunti G, Hu Y, Wendler F, DasGupta R, *et al.* (2006). Functional genomics reveals genes involved in protein secretion and Golgi organization. Nature 439, 604–607.

Benowitz LI, Routtenberg A (1997). GAP-43: an intrinsic determinant of neuronal development and plasticity. Trends Neurosci 20, 84–91.

Bonifacio JS, Glick BS (2004). The mechanisms of vesicle budding and fusion. Cell 116, 153–166.

Bormann P, Zumsteg VM, Roth LWA, Reinhard E (1998). Target contact regulates GAP-43 and α-tubulin mRNA levels in regenerating retinal ganglion cells. J Neurosci Res 52, 405–419.

Buniello A, MacArthur JAL, Cerezo M, Harris LW, Hayhurst J, Malangone C, McMahon A, Morales J, Mountjoy E, Sollis E, *et al.* (2019). The NHGRI-EBI GWAS Catalog of published genome-wide association studies, targeted arrays and summary statistics 2019. Nucleic Acids Res 47, D1005–D1012.

Burkhard SB, Bakkers J (2018). Spatially resolved RNA-sequencing of the embryonic heart identifies a role for Wnt/β-catenin signaling in autonomic control of heart rate. eLife 7, e31515.

Clark EM, Nonarath HJT, Bostrom JR, Link BA. (2020) Establishment and validation of an endoplasmic reticulum stress reporter to monitor zebrafish ATF6 activity in development and disease. Dis Models Mech 13.

Cronan MR, Rosenberg AF, Oehlers SH, Saelens JW, Sisk DM, Smith KLJ, Lee S, Tobin DM (2015). CLARITY and PACT-based imaging of adult zebrafish and mouse for whole-animal analysis of infections. Dis Model Mech 8, 1643–1650.

Diekmann H, Kalbhen P, Fischer D (2015). Characterization of optic nerve regeneration using transgenic zebrafish. Front Cell Neurosci 9, 118.

Fan J, Wang Y, Liu L, Zhang H, Zhang F, Shi L, Yu M, Gao F, Xu Z (2017). cTAGE5 deletion in pancreatic β cells impairs proinsulin trafficking and insulin biogenesis in mice. J Cell Biol 216, 4153–4164.

Ge L, Zhang M, Kenny SJ, Liu D, Maeda M, Saito K, Mathur A, Xu K, Schekman R (2017). Remodeling of ER-exit sites initiates a membrane supply pathway for autophagosome biogenesis. EMBO Rep 18, 1586–1603.

Gorur A, Yuan L, Kenny SJ, Baba S, Xu K, Schekman R (2017). COPII-coated membranes function as transport carriers of intracellular procollagen I. J Cell Biol 216, 1745–1759.

Hendee KE, Sorokina EA, Muheisen SS, Reis LM, Tyler RC, Markovic V, Cuturilo G, Link BA, Semina EV (2018). PITX2 deficiency and associated human disease: insights from the zebrafish model. Hum Mol Genet 27, 1675–1695.

Kabir MF, Kim H-R, Chae H-J (2018). Endoplasmic Reticulum Stress and Autophagy. Endoplasmic Reticulum, DOI:10.5772/INTECHOPEN.81381.

Kaneda M, Nagashima M, Nunome T, Muramatsu T, Yamada Y, Kubo M, Muramoto K, Matsukawa T, Koriyama Y, Sugitani K, *et al.* (2008). Changes of phospho-growth-associated protein 43 (phospho-GAP43) in the zebrafish retina after optic nerve injury: A long-term observation. Neurosci Res 61, 281–288.

Kim S-D, Pahuja KB, Ravazzola M, Yoon J, Boyadjiev SA, Hammamoto S, Schekman R, Orci L, Kim J (2012). SEC23-SEC31 the interface plays a critical role for export of procollagen from the endoplasmic reticulum. J Biol Chem 287, 10134–10144.

Kurokawa K, Okamoto M, Nakano A (2014). Contact of cis- Golgi with ER exit sites executes cargo capture and delivery from the ER. Nat Commun 5, 1–7.

Lang MR, Lapierre LA, Frotscher M, Goldenring JR, Knapik EW (2006). Secretory COPII coat component Sec23a is essential for craniofacial chondrocyte maturation. Nat Genet 38, 1198–1203.

Lee MCS, Miller EA, Goldberg J, Orci L, Schekman R. (2004). Bi-directional protein transport between the ER and Golgi. Annu Rev Cell Dev Biol 20, 87–123.

Lekszas C, Foresti O, Raote I, Liedtke D, König E-M, Nanda I, Vona B, Coster PD, Cauwels R, Malhotra V, *et al.* (2020). Biallelic TANGO1 mutations cause a novel syndromal disease due to hampered cellular collagen secretion. Elife 9, e51319.

Lemos RR, Oliveira DF, Zatz M, Oliveira JRM (2011). Population and computational analysis of the MGEA6 P521A variation as a risk factor for familial idiopathic basal ganglia calcification (Fahr's Disease). J Mol Neurosci 43, 333–336.

Liu M, Feng Z, Ke H, Liu Y, Sun T, Dai J, Cui W, Pastor-Pareja JC (2017). Tango1 spatially organizes ER exit sites to control ER export. J Cell Biol 216, 1035–1049.

Maeda M, Katada T, Saito K (2017). TANGO1 recruits Sec16 to coordinately organize ER exit sites for efficient secretion. J Cell Biol 216, 1731–1743.

Maeda M, Kurokawa K, Katada T, Nakano A, Saito K (2019). COPII proteins exhibit distinct subdomains within each ER exit site for executing their functions. Sci Re 9, 1–7.

Maeda M, Saito K, Katada T (2016). Distinct isoform-specific complexes of TANGO1 cooperatively facilitate collagen secretion from the endoplasmic reticulum. Mol Biol Cell 27, 2688–2696.

Maiers JL, Kostallari E, Mushref M, deAssuncao TM, Li H, Jalan-Sakrikar N, Huebert RC, Cao S, Malhi H, Shah VH (2016). The unfolded protein response mediates fibrogenesis and collagen I secretion through regulating TANGO1 in mice. Hepatology 65, 983–998.

Malhotra V, Erlmann P (2015). The pathway of collagen secretion. Annu Rev Cell Dev Biol 31, 109–124.

McCaughey J, Stephens DJ (2019). ER-to-Golgi transport: a sizeable problem. Trends Cell Biol 29, 940–953.

Melville DB, Montero-Balaguer M, Levic DS, Bradley K, Smith JR, Hatzopoulos AK, Knapik EW (2011). The feelgood mutation in zebrafish dysregulates

COPII-dependent secretion of select extracellular matrix proteins in skeletal morphogenesis. Dis Models Mech 4, 763–776.
Miller EA, Schekman R (2013). COPII—a flexible vesicle formation system. Curr Opin Cell Biol 25, 420–427.
Miyares RL, de Rezende VB, Farber SA (2014). Zebrafish yolk lipid processing: a tractable tool for the study of vertebrate lipid transport and metabolism. Dis Models Mech 7, 915–927.
Oliveira JRM, Sobrido MJ, Spiteri E, Hopfer S, Meroni G, Petek E, Baquero M, Geschwind DH (2007). Analysis of candidate genes at the IBGC1 locus associated with idiopathic basal ganglia calcification ("Fahr" Disease'). J Mol Neurosci 33, 151–154.
Omari S, Makareeva E, Roberts-Pilgrim A, Mirigian L, Jarnik M, Ott C, Lippincott-Schwartz J, Leikin S (2018). Noncanonical autophagy at ER exit sites regulates procollagen turnover. Proc Natl Acad Sci USA 115, E10099–E10108.
Petley-Ragan LM, Ardiel EL, Rankin CH, Auld VJ (2016). Accumulation of laminin monomers in *Drosophila* glia leads to glial endoplasmic reticulum stress and disrupted larval locomotion. J Neurosci 36, 1151–1164.
Pitman JL, Bonnet DJ, Curtiss LK, Gekakis N (2011). Reduced cholesterol and triglycerides in mice with a mutation in Mia2, a liver protein that localizes to ER exit sites. J Lipid Res 52, 1775–1786.
Raote I, Ernst AM, Campelo F, Rothman JE, Pincet F, Malhotra V (2020). TANGO1 membrane helices create a lipid diffusion barrier at curved membranes. eLife 9, e57822.
Raote I, Malhotra V (2019). Protein transport by vesicles and tunnels. J Cell Biol 218, 737–739.
Raote I, Ortega Bellido M, Pirozzi M, Zhang C, Melville D, Parashuraman S, Zimmermann T, Malhotra V (2017). TANGO1 assembles into rings around COPII coats at ER exit sites. J Cell Biol 216, 901–909.
Reynolds HM, Zhang L, Tran DT, Hagen KGT (2019). Tango1 coordinates the formation of ER/Golgi docking sites to mediate secretory granule formation. J. Biol. Chem. 295, 19498–19510.
Ríos-Barrera LD, Sigurbjörnsdóttir S, Baer M and Leptin M (2017). Dual function for Tango1 in secretion of bulky cargo and in ER-Golgi morphology. Proc Natl Acad Sci U S A 114, E10389–E10398.
Saito K, Chen M, Bard F, Chen S, Zhou H, Woodley D, Polischuk R, Schekman R, Malhotra V (2009). TANGO1 facilitates cargo loading at endoplasmic reticulum exit sites. Cell 136, 891–902.
Saito K, Yamashiro K, Ichikawa Y, Erlmann P, Kontani K, Malhotra V, Katada T (2011). cTAGE5 mediates collagen secretion through interaction with TANGO1 at endoplasmic reticulum exit sites. Mol Biol Cell 22, 2301–2308.
Saito K, Yamashiro K, Shimazu N, Tanabe T, Kontani K, Katada T (2014). Concentration of Sec12 at ER exit sites via interaction with cTAGE5 is required for collagen export. J Cell Biol 206, 751–762.
San B, Aben M, Elurbe DM, Voeltzke K, Den Broeder MJ, Rougeot J, Legler J, Kamminga LM (2018). Genetic and Epigenetic Regulation of Zebrafish Intestinal Development. Epigenomes 2, 19.
Santos AJM, Nogueira C, Ortega-Bellido M, Malhotra V (2016). TANGO1 and MIA2/cTAGE5 (TALI) cooperate to export bulky pre-chylomicrons/VLDLs from the endoplasmic reticulum. J Cell Biol 213, 343–354.
Sato K, Nakano A (2005). Dissection of COPII subunit-cargo assembly and disassembly kinetics during Sar1p-GTP hydrolysis. Nat Struct Mol Biol 12, 167–174.
Skene JHP (1989). Axonal growth-associated proteins. Annu Rev Neurosci 12, 127–156.
Stark C, Breitkreutz B-J, Reguly T, Boucher L, Breitkreutz A, Tyers M (2006). BioGRID: a general repository for interaction datasets. Nucleic Acids Res 34, D535–D539.
Townley AK, Feng Y, Schmidt K, Carter DA, Porter R, Verkade P, Stephens DJ (2008). Efficient coupling of Sec23-Sec24 to Sec13-Sec31 drives COPII-dependent collagen secretion and is essential for normal craniofacial development. J Cell Sci 121, 3025–3034.
Udvadia AJ (2008). 3.6kb genomic sequence from Takifugu capable of promoting axon growth-associated expression in developing and regenerating zebrafish neurons. Gene Expression Patterns 8, 382–388.
Walter P, Ron D (2011). The unfolded protein response: From stress pathway to homeostatic regulation. Science 334, 1081–1086.
Wang Y, Liu L, Zhang H, Fan J, Zhang F, Yu M, Shi L, Yang L, Lam SM, Wang H, *et al*. (2016). Mea6 controls VLDL transport through the coordinated regulation of COPII assembly. Cell Res 26, 787–804.
Watson P, Townley AK, Koka P, Palmer KJ, Stephens DJ (2006). Sec16 defines endoplasmic reticulum exit sites and is required for secretory cargo export in mammalian cells. Traffic 7, 1678–1687.
Westerfield M (1995). The zebrafish Book. Eugene, Oregon: University of Oregon Press.
White RJ, Collins JE, Sealy IM, Wali N, Dooley CM, Digby Z, Stemple DL, Murphy DN, Billis K, Hourlier T, *et al*. (2017). A high-resolution mRNA expression time course of embryonic development in zebrafish. eLife 6, e30860.
Wilson DG, Phamluong K, Li L, Sun M, Cao TC, Liu PS, Modrusan Z, Sandoval WN, Rangell L, Carano RAD, *et al*. (2011). Global defects in collagen secretion in a Mia3/TANGO1 knockout mouse. J Cell Biol 193, 935–951.
Yang B, Treweek JB, Kulkarni RP, Deverman BE, Chen C-K, Lubeck E, Shah S, Cai L, Gradinaru V (2014). Single-cell phenotyping within transparent intact tissue through whole-body clearing. Cell 158, 945–958.
Zhang F, Wang Y, Wang T, Yao L, Lam SM, Huang X, Fan J, Wang Q, Liu L, Jiang Y, *et al*. (2018). cTAGE5/MEA6 plays a critical role in neuronal cellular components trafficking and brain development. Proc Natl Acad Sci USA 115, E9449–E9458.